4 DiffMod7 – Modelling Oxygen Diffusion and Pyrite Decomposition in the Unsaturated Zone Based on Ground Air Oxygen Distribution

Henrik Hecht*, Martin Kölling and Norbert Geisler

Abstract

In the context of a project on pyrite weathering and the associated oxygen transport in the unsaturated zone of lignite open mining dumps a model for pyrite weathering in the unsaturated zone was developed from a simple model idea. It was validated in laboratory column experiments. The model allows the quantification of the processes occurring in the laboratory experiments and thus an identification of the relevant mechanisms, as well as the forecasting of the course of such experiments. A transfer to low complexity natural systems is possible by the simplicity of the model. With the help of the model, the oxygen penetration depth and the associated depyritization depth of a 43 years old dump body could be predicted and validated by in situ measurements of the oxygen distribution and by the determination of pyrite contents.

4.1 Introduction

Scientific investigations include the development of plausible model conceptions. In many cases these model conceptions lead to the development of computer models, which are – in the ideal case – not only able to describe the investigations made but can also be used for prognosis purposes. An important point associated with the development of such models is the identification of the relevant process-controlling parameters. The simpler these models are regarding computational effort and parameter scope, the easier they may be scaled up to large-dimensioned natural systems. Modelling of natural systems usually requires processing a large quantity of base data including a more complicated parameterization.

* Fachbereich 5 – Geowissenschaften, Universität Bremen, Postfach 330440, 28334 Bremen; e-Mail: hhecht@uni-bremen.de

Geochemical Processes: Conceptual Models for Reactive Transport in Soil and Groundwater. Research Report. Deutsche Forschungsgemeinschaft (DFG).
 ISBN: 978-3-527-27764-3

The degradation of pyrite with oxygen causes the release of very large quantities of iron and sulphuric acid. Successive reactions induced by pyrite weathering result in heavy metal release and both dissolution and formation of minerals. Sorption processes additionally entail strong modifications of the seepage water and groundwater chemistry. The basic mechanisms associated with pyrite weathering are reviewed in Evangelou (1995), Appelo and Postma (1994) and Nordstrom (1982). The initial cause of complex processes is the contact of pyrite with atmospheric oxygen when pyrite-bearing material is being exposed. In the investigations presented here, special attention was put on both the oxygen recharge and the pyrite turnover in the zone of reaction. The relevant processes are convective and diffusive oxygen transport as well as the pyrite reactivity (specific mineral surface, turnover rates).

In column experiments, convective transport processes were important only in the sense of gas volume recharge following oxygen consumption. Diffusive oxygen recharge was identified as the most important transport process. For the implementation in a model, different numerical solutions are available. In each case, the soil-physic characteristics (porosity, water content, tortuosity factor) determining the soil-specific diffusion coefficient have a crucial influence on the oxygen flux. Comprehensive reviews of transport modelling and soil-physic parameters are given e.g. by Boudreau (1997) and Grathwohl (1998). Since the characteristics of the pyrite grains are responsible for the direct interaction between pyrite and oxygen, the grain modification in the course of pyrite decomposition has a direct influence on oxygen fluxes and pyrite turnover. Therefore, the modification of pyrite grains must be considered.

Different approaches for modelling pyrite decomposition in the saturated and/or unsaturated zone of overburden material have been described in the literature. At present, the model developed furthest is probably the programme MINTOX (Wunderly et al., 1996), which couples linear oxygen diffusion, pyrite decomposition by means of a shrinking core model (Davis and Ritchie, 1986), geochemical equilibrium calculations and two-dimensional transport. A similar model concept was used by Gerke et al. (1998) for the calculation of acid mine drainage producing processes in lignite dumps. Prein (1994) developed the linear model SAPY for pyrite decomposition in lignite open mining dumps, which considers the relevant transport processes in the liquid and in the gaseous phase and which allows to calculate the distribution of the reaction products in different dump structures. Puura et al. (1999) developed a model for the atmospheric oxidation of pyrite bearing waste rock. It considers the calculation of the oxygen recharge in waste dumps and shale lumps containing sulfide minerals. Pyrite oxidation and carbonate buffering are calculated within a common reaction term. Xu et al. (2000) modelled pyrite oxidation and discrete event type processes under saturated and unsaturated conditions with the help of two transport reaction models in fractured rocks.

In the development of the model presented here, a focus was put on simple and plausible operability as well as a clear visualization of the processes. The effects of parameter modifications may be observed while the calculations are going on. The model is limited to processes identified as substantial in the systems examined, which drastically reduces calculation time. One aim was to show that even with a simplified model approach the major processes may be described and predicted.

4.2 Data Basis for Model Development

In a column experiment on pyrite decomposition in the unsaturated zone of overburden material of an open cast lignite mine both the column effluent and the soil gas oxygen content were monitored. The columns were constructed from perspex pipes with a diameter of 10 cm and a length of 85 cm. The columns were filled with overburden material from the open cast lignite mine Garzweiler, West Germany. The column was irrigated twice a day during total experiment duration of 600 days and sampled once a week. In the effluent solution the reaction products of pyrite decomposition and successive processes (sorption, solution, etc.) were determined. Along the soil profile in the column the progressing pyrite decomposition could be observed within the unsaturated zone by soil gas oxygen measurement with a modified optical measuring system (Microx 1, company Presens (www.presens.de), Holst et al., 1995). The pyrite-bearing overburden material was examined for both its soil-physical parameters (particle size distribution, water content, soil-specific diffusion coefficient) and chemical characteristics (pyrite content (chrome extraction after Volkov and Zhabina (1977)), elemental composition).

In the lower 20 cm of the column, no more open pore space is found due to increased water saturation. The pyrite in this zone is not involved in the alteration of the column in relevant quantities. The results of the parameters important for the model development are represented in Fig. 4.1. It shows the cumulative amount of the iron release over time and the associated development in the oxygen depth distribution during the depyritization. Additionally, the pyrite content in the ideally unsaturated area of the column is plotted. It is the pyrite quantity, which is available for reactions with diffusively transported oxygen.

Approximately a few days after the beginning of the experiment equilibrium between oxygen consumption and oxygen recharge is established. Subsequently, the oxygen penetrates more and more deeply into the column and thus reflects a progres-

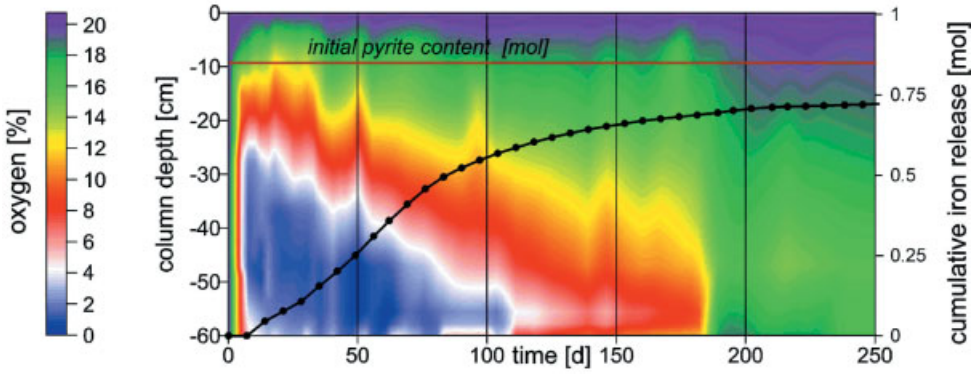

Figure 4.1: Pyrite decomposition in soil column experiment; development of oxygen depth distribution and cumulative amount of iron release over time; initial pyrite content.

sive depyritization of the material. After approximately 180 days, the oxygen concentration sharply increases throughout the column indicating the end of the pyrite decomposition process within the ideally unsaturated area of the column. The discharge of the primary reaction products iron and sulfate also reflects the processes in the column. The initial discharge solution is characterized by washout of pyrite weathering products that have been formed in the material prior to the beginning of the experiment. Within the first hundred days the release of iron and sulfate becomes nearly constant. This is controlled by the approximately constant pyrite degradation on the column. After 100 days the release slightly decreases as the front of the active pyrite decomposition zone reaches the lower end of the column. After approximately 200 days the majority of the reaction products released within the unsaturated area of the column have been washed off the column. The subsequent residual release of pyrite oxidation products is characterized by reduced oxygen availability in the lower nearly water-saturated part of the column.

4.3 The Model (DiffMod7)

4.3.1 Model Concept

The data obtained in the column experiments form the basis for the development of a model for pyrite decomposition in the unsaturated zone. The model was programmed in Visual Basic 6. Visual programming languages allow a quick and easy way of establishing an intuitive graphical user interface, which provides a graphical control of the model calculations at runtime. The model presented here is an iterative cell model, which calculates the diffusive oxygen recharge and the oxic pyrite decomposition in the unsaturated zone. A simple transport of the reaction products with the seepage water is integrated into the model. No special attention is paid to diffusive/dispersive effects in the liquid phase or on secondary mineral reactions which are not included in the present state of the model.

4.3.1.1 Diffusive Transport

A pyrite decomposition process is an instationary process since the solid phase reactant is being consumed under pyrite-oxidizing conditions causing changes in both reactive surface and mineral mass. Only in a fictitious system, in which the velocity of the depyritization front penetration by chance equals the surface erosion stationary conditions may be found. Diffusion under instationary conditions may be described by numerical solutions of the transport reaction equation considering Ficks second law. Reactions can be integrated quite simply, if transport and reaction are decoupled in a

combined mixing cell/analytical model (Schulz and Reardon, 1983). Equation (1) shows the diffusion/dispersion part of the explicit solution of the transport reaction equation (e.g. Boudreau, 1997) used in our model. In DiffMod7, convective oxygen recharge resulting from the loss in gas volume is not calculated within the transport reaction equation. The reaction term is separated as well. The advantage of the procedure is that for the calculation of the new concentrations only the concentrations in the previous time step must be known.

$$C_t^1 = C_{t-\Delta t}^1 + \Delta t \cdot D_{sed} \cdot \left(\frac{C_{t-\Delta t}^2 - 2 \cdot C_{t-\Delta t}^1 + C_{t-\Delta t}^0}{(\Delta x)^2} \right) \tag{1}$$

C_t^1 calculated concentration in the regarded cell [mol m^{-3}],

$C_{t-\Delta t}^1$ concentration of the regarded cell in the previous time step [mol m^{-3}],

$C_{t-\Delta t}^0$ concentration of the previous cell in the previous time step [mol m^{-3}],

$C_{t-\Delta t}^2$ concentration of the next cell in the previous time step [mol m^{-3}],

D_{sed} soil-/sediment-specific diffusion coefficient [mol m^{-2}s^{-1}] (Eq. (3)),

Δt time step [s],

Δx cell height [m].

Equation (1) is stable only for certain combinations of Δt and Δx (e.g. Mitchell and Griffiths, 1980). The condition, which has to be met in order to prevent oscillations within the calculation, reads:

$$\Delta t \leq \frac{(\Delta x)^2}{2 \cdot D_{sed}} \cdot \tag{2}$$

The soil-specific diffusion coefficient is the diffusion coefficient corrected for the soil-physic parameter tortuosity (θ) in free air (e.g. Boudreau, 1997).

$$D_{sed} = \frac{D_0}{\theta^2} \tag{3}$$

D_0 pressure- and temperature-corrected diffusion coefficient in free air.

The tortuosity describes the ratio of the (average) incremental distance that an ion/molecule must travel to cover the direct distance in the direction of diffusion (Berner, 1980) and is thus the factor, which describes the increase in travel distance in the porous medium. Since the definitions of tortuosity in literature indicate small however substantial differences (an excellent overview of different procedures, equations and definitions is given by Boudreau (1997)), the definition used here is described briefly. The diffusion coefficient is corrected by the squared tortuosity. The square of the tortuosity is called tortuosity factor (Carman, 1937). This factor represents the

entire correction factor for the calculation of the soil-specific diffusion coefficient from the diffusion coefficient in free air (Boudreau, 1997). The tortuosity factor is not a measurable parameter. It may be calculated from empirical equations. Within the model, Eq. (4) is used for the calculation of the tortuosity factor from the diffusion-effective porosity (φ_e). It results in a good general solution for fine-grained sediments (Boudreau, 1997).

$$\theta^2 \approx 1 - 2 \cdot \ln(\varphi_e) = 1 - \ln(\varphi_e^2) \tag{4}$$

The soil-physical parameters in natural systems vary with depth. A weighting of the parameters of the interacting cells has to be integrated into the calculation of the diffusive flux with the explicit solution (e.g. Landenberger, 1998). Equation (5) shows the equation used for the calculation of the oxygen concentration in DiffMod7. The topmost and the bottommost cell of the model are calculated separately in consideration of upper and lower boundary conditions.

$$C_t^1 = C_{t-\Delta t}^1 + \frac{\Delta t \cdot D_0}{2 \cdot \Delta x^2} \cdot \left[\left(\frac{1}{\theta_1^2} + \frac{1}{\theta_2^2} \right) \cdot \left(C_{t-\Delta t}^2 - C_{t-\Delta t}^1 \right) - \left(\frac{1}{\theta_0^2} + \frac{1}{\theta_1^2} \right) \cdot \left(C_{t-\Delta t}^1 - C_{t-\Delta t}^0 \right) \right] \tag{5}$$

θ_0^2 tortuosity factor previous cell,

θ_1^2 tortuosity factor current cell,

θ_2^2 tortuosity factor next cell.

4.3.1.2 Pyrite Weathering

In the model DiffMod7 the diffusion of oxygen within the unsaturated zone is calculated considering weighted soil-specific parameters according to the stability criteria. After each time step for which the diffusive flux between the cells was calculated, the oxygen consumption by pyrite oxidation is determined for this time interval. The oxygen consumption is calculated as a function of the pyrite quantity available, the pyrite grain surface and the pyrite oxidation rate. The reaction equation forming the basis for pyrite decomposition within the model reads:

$$FeS_2 + \tfrac{15}{4} O_2 + \tfrac{1}{2} H_2O \leftrightarrow Fe^{3+} + 2SO_4^{2-} + H^+ \tag{6}$$

Due to the oxidation process, the pyrite quantity within a cell decreases with time, while the specific pyrite grain surface increases by the slow decrease in grain size during the decomposition. The increase of the specific surface is implemented as function of the pyrite quantity according to Eq. (7).

$$A_{py}^t = \sqrt[3]{\frac{m_{py}^{t_0}}{m_{py}^t}} \cdot A_{py}^{t_0} \tag{7}$$

A_{py}^{t} current specific surface of the pyrite in cell,

$A_{py}^{t_0}$ initial value of the specific surface of the pyrite,

m_{py}^{t} current pyrite quantity in cell,

$m_{py}^{t_0}$ initial value of the pyrite quantity in cell.

4.3.1.3 Convective Transport

Convective gas phase transport in natural unsaturated soil systems may be induced by variations in temperature, air pressure and groundwater, by wind pressure or by seepage water movement after rain events. All these processes are of minor importance in lab column experiments and have not been implemented in DiffMod7. The only convective movement in the gaseous phase considered in DiffMod7 is the ground air recharge due to gas volume decrease caused by oxygen consumption. The effects of this type of convection have to be taken into consideration as they result in an increase of the initial oxygen penetration depth or the thickness of the pyrite oxidation zone and thus induce an increase of the total pyrite decomposition rate on the column by 10 to 15 %.

The seepage transport of the reaction products in DiffMod7 is only determined by the seepage velocity. Secondary mineral reactions that might affect the transport by transfer of reaction products from liquid phase into solid phase are neglected.

4.3.2 Computer Implementation of Model and User Interface

Figure 4.2 shows the user interface of the model. Basic input parameters are the total depth, the model surface area, the density and the overall porosity of the material and its pyrite content, the pyrite grain surface or a pyrite grain size, a pyrite oxidation rate and the infiltration. Since the programme was originally developed for the modelling of column experiments, these input parameters are not variable with depth. The tortuosity factor, the diffusion-effective porosity and the initial oxygen concentrations may vary with depth and may be individually input for each cell. The uppermost cell represents the ambient air. The lower boundary is defined by a zero gradient condition. Checking the “no convection” control button can deactivate the convective transport described above. The input of the model time step duration is automatically validated for meeting the stability criteria. In addition to the total model time the time steps after which intermediate values of oxygen concentration, pyrite content, pyrite surface, pyrite decomposition and seepage water concentration in each cell are stored in a result file. These values allow the plotting of time-depth distributions of these parameters after the model run. During the model calculation the oxygen concentration, the pyrite quantity and the pyrite decomposition over depth are displayed as diagrams on the right side of the user interface. The maximum of the x-axes is scaled automatically to ambient air oxygen, the initial pyrite content and the initial pyrite decomposition. The

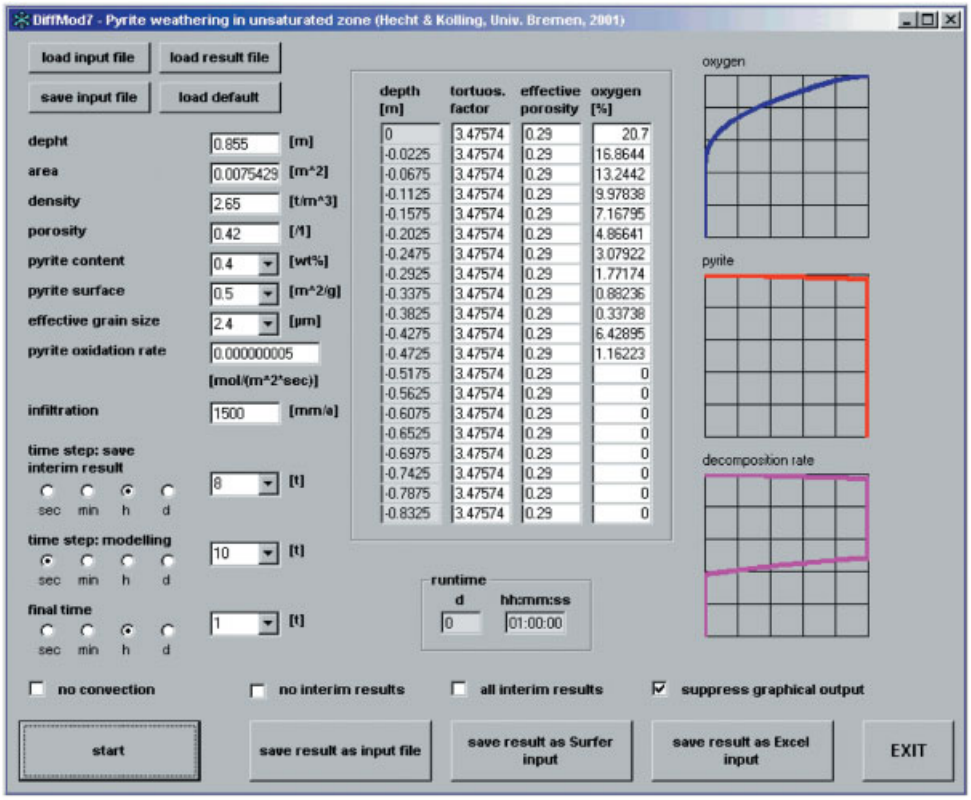

Figure 4.2: DiffMod7 – Graphical user interface.

graphical representation of intermediate results at runtime very well illustrates the processes going on, yet calculations may be strongly accelerated by checking the "suppress graphical output" control if needed. The screen output then reduces to updating the elapsed model time. The start conditions of each model run may be saved in an input file. The results of the model run along with all intermediate results can be stored as data sets compatible with Excel or Surfer.

4.3.3 Example

Figure 4.3 shows an example of a model run with appropriate start parameters. Equilibrium between oxygen consumption and oxygen recharge is quickly established on the column indicated by a stable oxygen depth profile. The graphs of pyrite oxidation rates show that initially throughout the oxygen penetration depth equal amounts of oxygen are consumed by the pyrite oxidation due to uniform initial amounts of available pyrite surface.

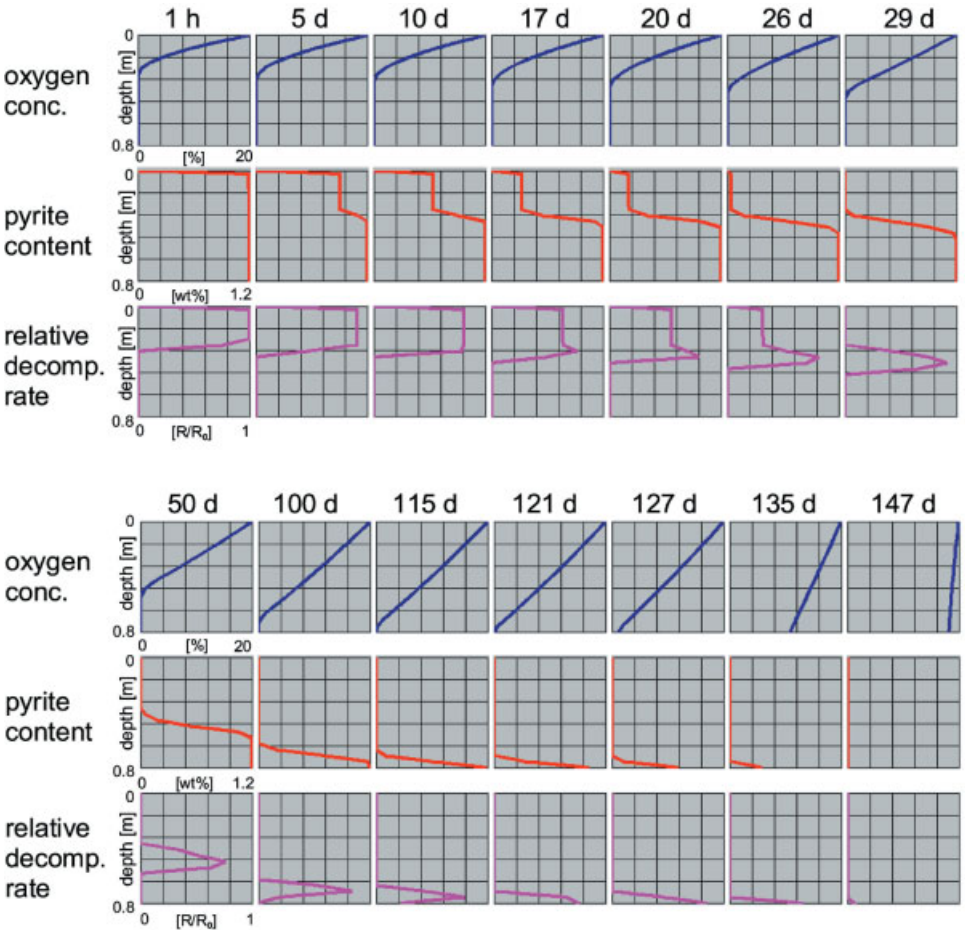

Figure 4.3: Example model run. Graphical output DiffMod7 during calculation. Start parameters: pyrite content: 1.2 wt.%; specific pyrite surface: 1 [m^2g^{-1}]; pyrite oxidation rate: 5×10^{-9} [mol $m^{-2}s^{-1}$]; effective porosity: 0.29; tortuosity factor: 3.33.

The broad zone of equal decomposition rates remains existing until the entire pyrite is weathered (29 days). During this period the pyrite quantity in this zone slowly decreases and the decomposition rate decreases such that oxygen may gradually penetrate further down into the unweathered material. The change from a mainly surface controlled to a mainly diffusion controlled process is indicated by the evolution of a reaction front which plots as a peak in decomposition rates and which is also indicated in the pyrite depth distribution by a sharp separation of a pyrite-free upper layer and a lower layer with initial pyrite content. After 29 days the uppermost part of the model system is depyritized and the reaction front starts moving further down into the sediment. Due to decreasing fluxes caused by increasing diffusion distances from the surface to the reaction front, both the decomposition rates and the thickness of the reac-

tion front decrease with time. The maximum decomposition rates are not found in the cell with the highest pyrite content, but in the cell above since only there sufficient quantities of oxygen are available. The reaction front slowly moves into the sediment, until the entire pyrite has been consumed. After approximately 150 days the decomposition process is finished, so that in all depths ambient air oxygen concentration is achieved.

One remarkable result of this model calculation is the shape of the oxygen depth profiles. Although at the beginning of the model calculation the reaction rates throughout the entire oxygen penetration depth are constant, the oxygen profiles are only slightly curved. The interpretation of an oxygen profile of this kind as presented e.g. in Schulz (2000) would assume rather low reaction rates in the upper part of the sediment column and the main reaction zone would be expected where the oxygen-depth curve shows an increased curvature. Starting from the 29th day the oxygen almost linearly decreases with depth indicating oxygen flux into a sink located at the depth where the oxygen concentration becomes zero. The reaction front is remarkably wider than the zone of change in the slope of the oxygen depth distribution seems to be. The change in slope is reflected in the decomposition rates, which are in interaction with the change in oxygen concentration differences. In this model run, the oxygen profiles also reflect the effects of convective oxygen transport. After the uppermost layer of the column has been depyritized, the oxygen-depth distribution changes from a concave to a convex shape. This effect is caused by the superposition of diffusive oxygen recharge and the convective recharge caused by the decrease in gas volume (transition of oxygen from the gaseous phase to the liquid species sulfate). The gas volume loss in the reaction zone causes a convective downward shift of ground air. The type of convection considered here thus characteristically modifies the shape of the oxygen profile and the associated oxygen flux. As described above additional modifications of the oxygen depth distribution by convection may occur in natural systems.

4.3.4 Modelling Column Experiments

The input parameters necessary for the modelling of the column experiment described in Section 4.2 are well known from analysis of the column material and from the experimental boundary conditions except for the tortuosity factors, which cannot be measured directly. In this case, they are calculated according to Eq. (4). Additionally, the parameters pyrite grain surface and pyrite oxidation rate, which are initially difficult to determine for natural material, are necessary for modelling. An oxidation rate of 7×10^{-9} [mol $m^{-2}s^{-1}$] has been assumed. Kölling (1990) found oxidation rates in this order of magnitude for pyrite decomposition processes under ideal conditions catalysed by *Thiobacillus ferrooxidans*. Values for the grain size of early diagenetically formed pyrites within the overburden material are given in Friedrich et al. (1999). A good estimate for the specific surface is 0.5 [$m^2\,g^{-1}$], assuming some grain roughness. Finally, adjusting these two parameters leads to a fit of the modelled oxygen time-depth distribution to the measured data. The results are presented in Fig. 4.4. The

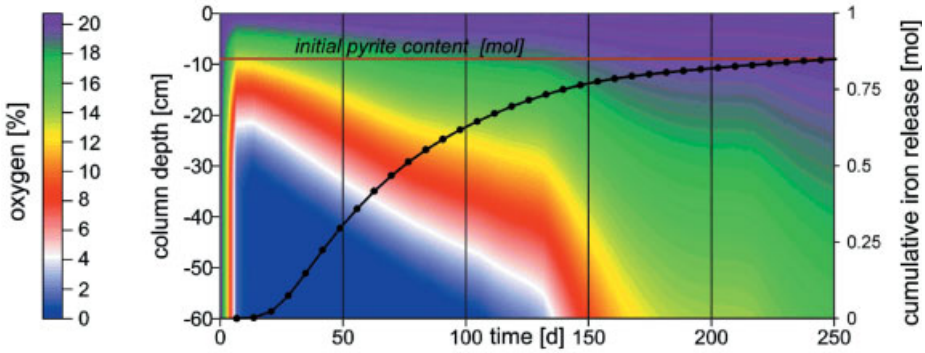

Figure 4.4: Modelled oxygen time-depth distribution and cumulative iron release during pyrite decomposition in column experiment (compare experimental data in Figure 4.1).

measured oxygen time-depth distribution is very well reflected in the model calculation for the uppermost 60 cm of the column (ideally unsaturated area). In the lower area of the column (not ideally unsaturated) pyrite decomposition characterized by low oxidation rates continues for a very long time. The model calculation yields a discharge of reaction products with the seepage water, which corresponds with the measured values of the column experiment (compare Fig. 4.1). The similarity of measured and predicted discharge may serve as an independent validation of the model indicating that the major processes are obviously implemented at a reasonable accuracy level. The differences between observed and modelled iron discharge are affected by the precipitation of secondary iron bearing minerals (Hecht and Kölling, accepted) which have not been considered in this model.

The model calculation additionally yields results on the time depth distribution of pyrite decomposition rates, pyrite contents and the reaction product concentration in the seepage water (Fig. 4.5). The decomposition rate plot clearly shows the formation of the initial pyrite decomposition zone in the uppermost 30 cm of the column. Within this area the decomposition rates are limited mainly by the pyrite grain surface available so that a maximum decomposition is established which is uniform at all depths throughout this zone due to the sufficient oxygen supply. The decomposition rate in this zone decreases with time caused by the decrease of the pyrite quantity. The decrease in decomposition rates is slower than determined only by the decrease in pyrite quantity due to the simultaneous reduction of grain size and increase in specific grain surface. The reduced oxidation rates allow the oxygen to penetrate into deeper areas of the sediment column resulting in the formation of a pyrite oxidation front. The maximum in the decomposition rate depth distribution (green area) decreases with time as the reaction front proceeds into the sediment. At the lower end of the unsaturated part of the column the decomposition rate reduces to 75 % of the maximum rate due to the diffusively controlled oxygen recharge. The fluctuations within the turnover rates result from the spatial resolution of the model and are not the result of oscillations.

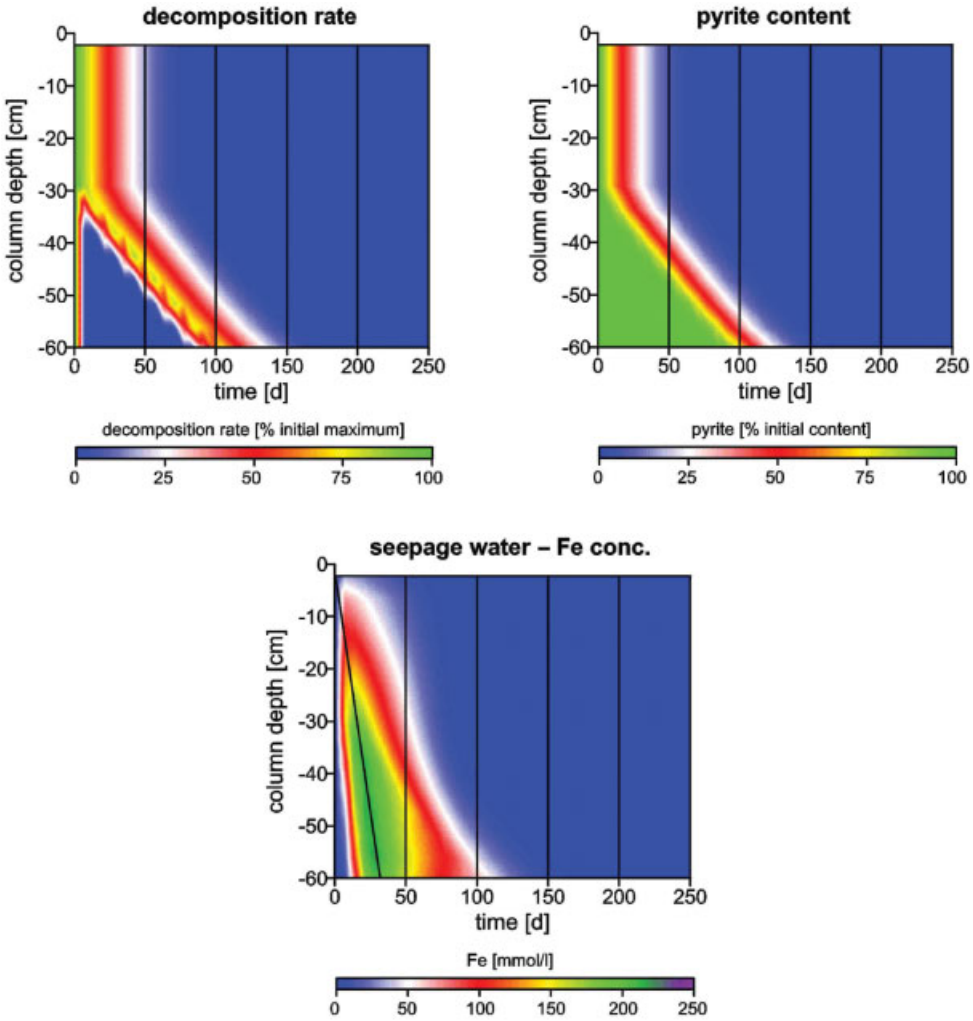

Figure 4.5: Modelled time-depth distribution of pyrite decomposition rates, pyrite contents and reaction product concentrations in the seepage water.

The depth-time distribution of the pyrite content also shows the depyritization. The comparison of the decomposition rates with the pyrite content plots reveals that initially a sufficient amount of pyrite is available in the lower part of the sediment. However, no pyrite oxidation occurs, since oxygen is consumed in the upper layers. The depth-time distribution of the seepage water concentrations results from the seepage water velocity, the pyrite decomposition rate and the velocity with which the reaction front moves downward. The position of a water particle with a constant seepage water velocity plots as a straight line in the time depth diagram. The edge of the high seepage water concentration area in space and time is determined by seepage water

velocity. Since a constant seepage water velocity has been assumed the high concentration seepage waters proceed linearly. Maximum seepage water concentrations are found in the water which has been at the top of the uppermost reaction zone at the start of the experiment since on its way down this water travels through the layers with the highest decomposition rates for the maximum duration. The solid line in Fig. 4.5 (bottom) marks this water. The temporal change in concentration at a given depth is characterized by a sharp increase as the edge of the plume reaches the depth of interest followed by a continuous decrease. In the lower part of the sediment the velocity of depyritization determines the shape of the back flank of the high concentration area in space and time. The fact that during the first 50 days a broader zone of fairly high concentrations evolves in the upper part of the sediment is caused by the uniformly high decomposition rates in the initially broad decomposition zone. In a larger system closer to natural conditions the characteristics of the distribution of pyrite weathering products in depth and time are pronounced more strongly.

4.3.5 Running Scenarios

The sensitivity of the model system to variations in the individual parameters can be checked easily using the computer model. One advantage is the possibility of checking different strategies to prevent pyrite oxidation for their efficiency. In the following examples, the final fit parameters for modelling the column experiment were used as base values. At first, the relevance of the soil-physical parameters should be considered. Effective porosity and tortuosity are in direct relation to each other. A change in effective porosity causes a change in tortuosity. Regarding this interaction, the effect on the diffusively controlled pyrite decomposition is more pronounced. Nevertheless, the effects of changes in these two parameters will first be regarded separately.

Halving the diffusion-effective porosity over the entire model depth results in a decrease of initial pyrite decomposition to approximately 60 to 70 % (compare Fig. 4.6). In the uppermost layer the oxygen supply is sufficiently large. The decomposition rate is the same as the result of the original calculation. Initially, the downward oxygen flux decreases to 50 % due to the bisected diffusion-effective cross section. However, the reduced oxygen flux is balanced by a reduced volume to be filled resulting in exactly the same concentration distribution as before. Without oxygen consumption the oxygen flux is bisected when the porosity is bisected. The oxygen consumption results in steeper gradients of oxygen concentration, consequently increasing oxygen flux to over 50 % of the original flux.

The discharge curve shows the characteristics of the different stages of pyrite decomposition inside the model column more clearly. At first, no discharge takes place, because the reaction products formed within the upper layer of the column are transported with the seepage water to the outlet. This first stage is followed by a period of constantly high discharges, which reflects the pyrite decomposition in the uppermost layers close to the surface. The third stage is a decrease of discharge, after the wide superficial oxidation zone has become pyrite-free and the main release occurs in

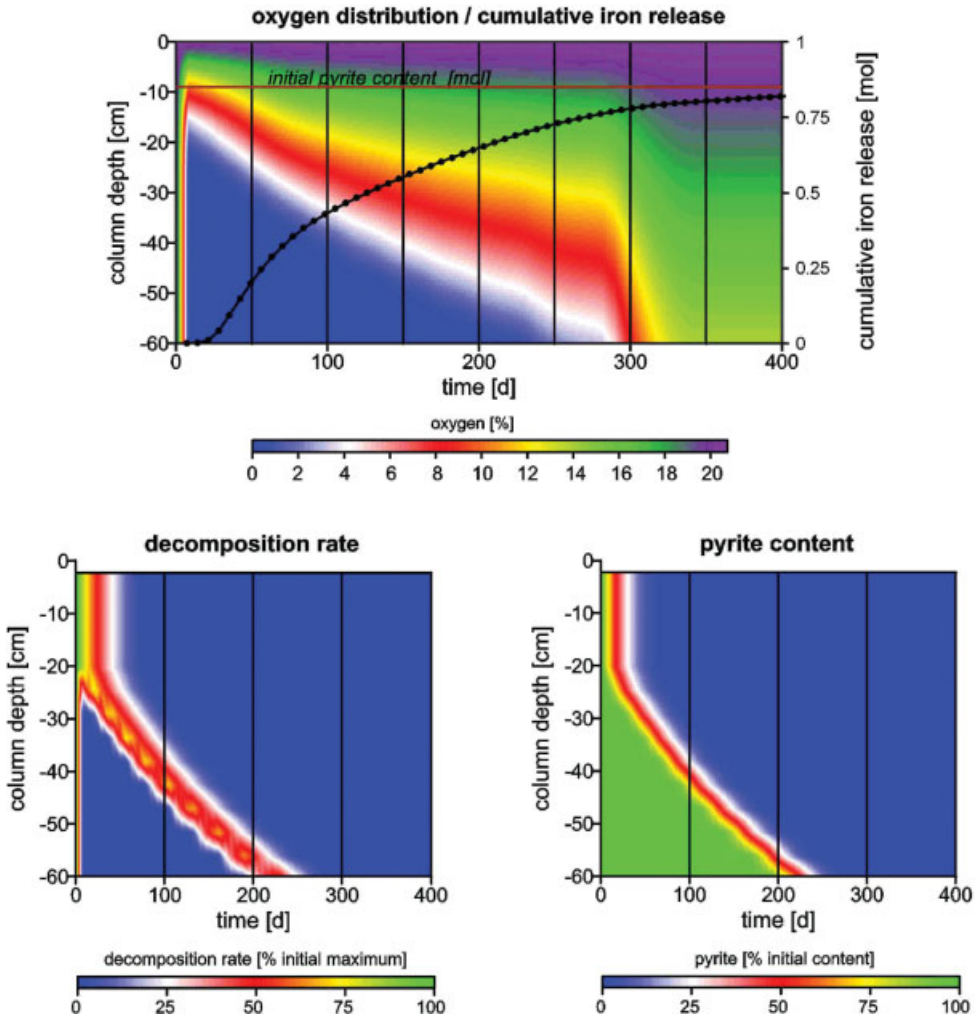

Figure 4.6: Modelled time-depth distribution of oxygen concentrations, pyrite decomposition rates and pyrite contents; cumulative iron release; bisected diffusion-effective porosity with regard to modelled column experiment; (same effect as duplication of tortuosity factor).

a narrow pyrite oxidation front, which is slowly proceeding downwards. With increasing distance of the oxidation front from the surface the oxygen gradient decreases causing a decrease in release rates. Another steep decrease in discharge occurs when the pyrite oxidation front reaches the lower not ideally unsaturated zone of the model system. After this point in time, there is no oxygen limitation in the unsaturated zone (oxygen is found in all depths), but a limitation by the residual pyrite surface. After the upper zone of the column has become completely pyrite-free the discharge is nearly terminated.

On the other hand, doubling the effective porosity leads to exactly inverse effects. The initial pyrite turnover rises to 150 % of the reference turnover.

Doubling the tortuosity factor while maintaining porosity apparently causes the same effects as halving the porosity while maintaining the tortuosity factor (Fig. 4.6). The modification results in halving the soil-specific diffusion coefficient, i.e. the initial flux is halved. However, since the open pore volume remains the same, the resulting concentrations are smaller, thus gradients become steeper. Overall, this results in oxygen fluxes that are larger than 50 % of the flux in the reference system. When oxygen is consumed by pyrite oxidation, the gradients continue to increase up to values between 60 and 70 %. Halving the tortuosity factor causes the opposite effect, resulting in an increase of the initial pyrite turnover to 150 % of the reference value.

If the relation between effective porosity and tortuosity factor is taken into consideration and the two parameters are modified accordingly, the resulting total change in turnover is the product of the two single changes in turnover. Halving the porosity coupled with duplication of tortuosity factor results in a decrease of initial flux to approximately 50 % (Fig. 4.7) of the reference flux.

For the examined systems, an approximated factor results that describes the total change in flux according to the change in tortuosity factor and effective porosity:

$$F = \sqrt{\frac{\theta_s^2 \cdot \varphi_e^v}{\theta_v^2 \cdot \varphi_e^s}} \tag{8}$$

F flux change factor,

θ_s^2 tortuosity factor – base value,

θ_v^2 changed tortuosity factor,

φ_e^s effective porosity – base value,

φ_e^v changed effective porosity.

Since porosity and tortuosity factor are coupled according to Eq. (4), the correct effect of change in porosity regarding the associated change in tortuosity factor may be calculated by combining Eqs. (4) and (8). The resulting equation reads:

$$F_\varphi \approx \sqrt{\frac{(1-2\ln(\varphi_e^s)) \cdot \varphi_e^v}{(1-2\ln(\varphi_e^v)) \cdot \varphi_e^s}} \tag{9}$$

F_φ coupled change in flux factor as a function of effective porosity for fine-grained sediments (after Eq. (4)).

The model calculations show that the soil-physical parameters strongly influence the pyrite decomposition rates and the discharge since these parameters have a direct impact on the amount of transported oxygen. Any change in the characteristics of oxygen transport will result in the change of the pyrite decomposition. While the total potential of acid production remains unchanged, the duration of pyrite weathering processes changes.

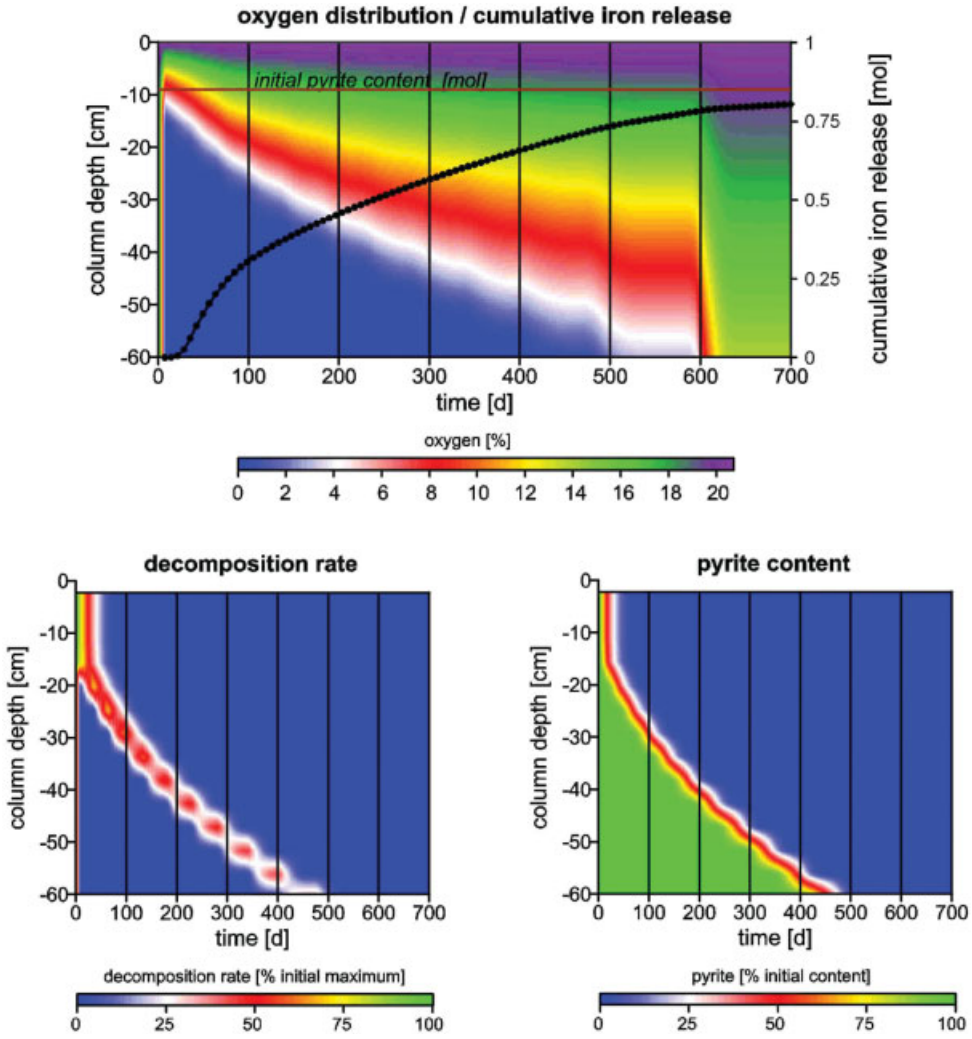

Figure 4.7: Modelled time-depth distribution of oxygen concentrations, pyrite decomposition rates and pyrite contents; cumulative iron release; halved diffusion-effective porosity and coupled duplication of tortuosity factor with regard to modelled column experiment.

A halving of the specific pyrite surface or the pyrite oxidation rate is associated with little effects on the turnover of pyrite and the discharge of reaction products. Both parameters have the same influence, because they both determine the pyrite turnover in moles per time and mass. The effect of halving the parameters (compared to the reference calculation) on the oxygen time-depth-distribution and the discharge is shown in Fig. 4.8.

It is shown that initial turnover and discharges remain almost unchanged, even though the oxygen distribution is strongly affected (doubled penetration depth). Since

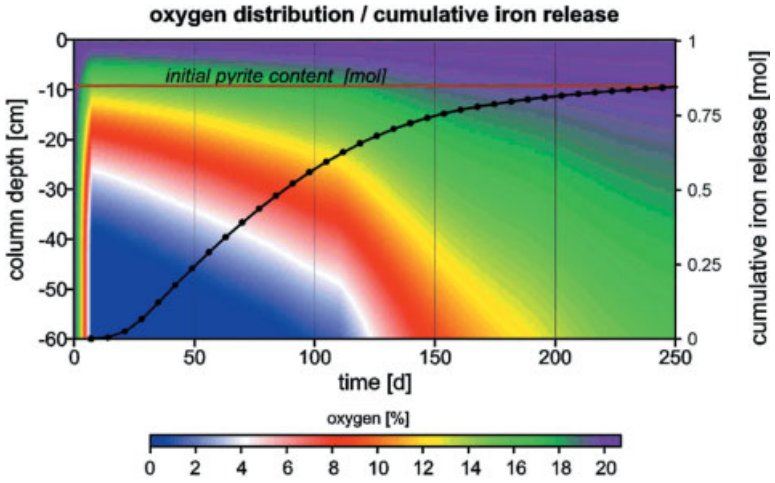

Figure 4.8: Modelled oxygen time-depth distribution and cumulative iron release; changes with regard to modelled column experiment. Halved pyrite oxidation rate (resp. specific pyrite surface).

the pyrite surface and the oxidation rate affect only the thickness of the pyrite oxidation front, in large natural systems the modifications result in a slight shift in depth distribution of reaction products. Doubling the specific pyrite surface or the pyrite oxidation rate causes a halved penetration depth, without great effects on pyrite decomposition and discharge of reaction products.

Modifying the pyrite content of the material has a strong influence on the total turnover of the system. Maintaining all other parameters constant, a duplication of the pyrite quantity results in doubling of the reactive surface, causing a 50 % decrease in the initial oxygen penetration depth (compare Fig. 4.9). The maximum concentrations, indicated by the increased gradient of the discharge curve, are only slightly larger than in the reference calculation. However, due to the increased pyrite quantity the release persists twice as long. The thickness of the pyrite decomposition front is half as thick as in the reference calculation and the time needed for a certain section of the system to become pyrite-free is doubled. The duration of the release of reaction products and their discharge is doubled whereas the seepage water concentration is similar to the reference results. The different stages of the discharge curve show the same features as the curve for halved permeability (Fig. 4.6), since this also results in a smaller thickness of both the initial pyrite weathering zone and the decomposition front.

The effect of halving the pyrite content is inverse. The total potential of acid production is halved as well as the reactive pyrite surface. Thus, the oxygen initially penetrates twice as far into the system. Compared to the reference system the concentrations are slightly smaller, but the total depyritization is completed twice as fast.

Therefore a modification of the pyrite content has strong effects on the time-depth distribution of oxygen and the total potential of acid production. The maximum concentrations in seepage water are not affected significantly.

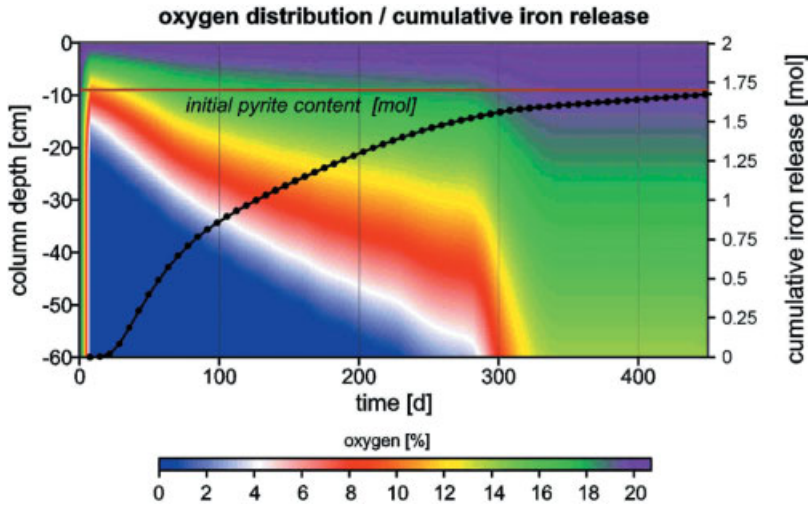

Figure 4.9: Modelled oxygen time-depth distribution and cumulative iron release. Duplication of pyrite content.

4.3.6 Field Test

The experience gained from column experiments was transferred to field scale. An approximately 43 year old dump body in the Lower Lusatian lignite district was chosen in order to examine the depyritization that has occurred already, and to predict the potential formation of acid mine drainage that remains. The investigations were carried out south of the residual lake 111 in a tailing of the abandoned open cast lignite mine Plessa, Germany, which has been dumped in 1956/57. In this mine, the world's first conveyor belt bridge was installed in 1929. This mining technique results in a rib structure of the tailings that is typical for the East German lignite-mining district (Klein, 1935). The dewatering of the open pit mine was stopped in 1959, after the mine had been closed in 1958, and the conveyor belt bridge was torn down.

At first, the model was used to predict the position of the depyritization front within the unsaturated zone. With estimates for the pyrite content of the material (mean approximately 1 [wt.%], personal communication) and the effective porosity (approx. 0.3, Hüttl et al., 2000) a first model calculation was executed. The result indicated a depyritization depth of approximately seven meters. In a field test, a well was sunk to a depth of 7.8 m and samples were taken from every meter. In the borehole, an array of optical oxygen sensors was installed with a sensor-to-sensor distance of one meter. After filling the borehole, quasi-stable conditions in oxygen distribution were reached already after 3.5 h (Fig. 4.10). The oxygen concentration decreases from 20.7 % (ambient oxygen) to values of 3–4 % at a depth of 6 to 8 m. The continuous decrease indicates that oxygen consumption at this depth is causing a recharge flux into this layer. The oxygen distribution by itself does not allow the prediction in which zone exactly

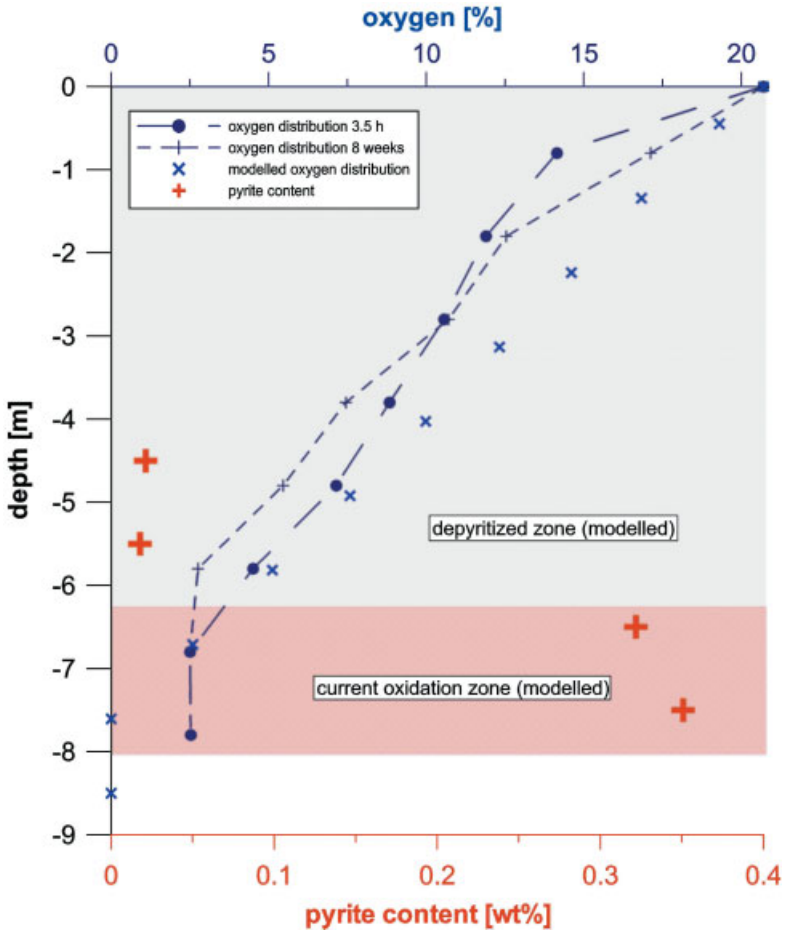

Figure 4.10: Measured oxygen and pyrite distribution in approx. 43 years old pyrite bearing dump body; modelled oxygen distribution, current oxidation zone and depyritization depth.

oxygen consumption takes place (cf. Section 4.3.3). The model conception implemented in DiffMod7 allows the interpretation of the profile regarding its emergence over time and the identification of the current pyrite oxidation zone and the depyritization depth (Fig. 4.10). The measurements immediately after installation of the sensors show that the first prediction of depyritization depth of approx. 7 m is reasonable.

The fact that measured oxygen concentrations do not decrease to zero is not clarified yet. However, the general shapes of the oxygen profiles – especially the parts where gradients change – remain untouched. The second measurement approximately 8 weeks after installation of the sensors revealed that the oxygen depth distribution had not changed significantly (Fig. 4.10). Higher concentrations were found in the uppermost layers. This is probably due to lower microbial activity in the upper soil resulting from lower ambient temperatures (Schachtschabel et al., 1992) during the measure-

ment eight weeks after installation of the sensors (temp. difference: 6 °C). In the lower part of the profile, oxygen concentrations had equilibrated with the surrounding gaseous phase. Oxygen concentrations were constantly low below a depth of 5.8 m. The initial model run could be refined using a better approach to the soil-physic parameters and the measured oxygen concentrations. The resulting modelled oxygen depth distribution matches the measured depth distribution (Fig. 4.10). Soil samples from below 6 m contain significant amounts of pyrite (0.3–0.4 wt.%) whereas the upper layers are pyrite-free (Fig. 4.10). Using the initial and current pyrite distribution data and the current oxygen distribution, the residual oxidation potential of the tailing and the release of reaction products over time may be modelled.

The seepage water concentrations that result from the model calculation are a worst-case prediction, as secondary mineral reactions are not included in DiffMod7. Neglecting buffer reactions does not introduce a great error in this case, because the acid neutralizing capacity of the overburden material is very low.

The processes included in the model calculation seem to be sufficient to explain the observed data, although convective gas transport by groundwater fluctuations, wind pressure, infiltration, air pressure changes as well as variations in temperature are not integrated in the model. This is due to different facts. The sampling point is located in a small forested plain, which is – in contrast to open dumps – not exposed to heavy wind pressure (see Section 4.4). During the operation of the mine, the ground water table was lowered by approximately 20 m. The dewatering was stopped one year after the mine was closed; another nine years later quasi-stable groundwater conditions had been reached (personal communication). At the sample location, groundwater recharge and fluctuations of the water table are small, and flow velocities are low (Hüttl et al., 2000). Thus, significant convective gas movement is not induced by these processes.

4.4 Discussion

The simulations presented above indicate that the basic processes of diffusive oxygen recharge and oxygen consumption in systems affected by pyrite oxidation are well implemented in DiffMod7. Some of the processes that have been neglected so far are of minor importance for the simulation results, whereas others should be subject to future improvements of DiffMod7:

There are various processes that induce convective gas transport that have not been considered, yet. Their impact on gas transport in soil is generally low (Wild, 1993). After Mattheß (1991), the proportion of gas exchange in the unsaturated zone that is caused by seepage water movement and subsequent displacement of ground air is in the range of 1/12 to 1/16 of the total gas exchange. Mattheß (1991) gives a value of 1/1000 of the total gas exchange for wind pressure effects in natural systems. Variations in ambient air pressure cause ground air movement. After Farrier and Massmann

(1992), ambient air pressure regionally varies slightly around an average value. The shift of ground air is quickly balanced by diffusive processes. The effects of water table fluctuations are similar to those of air pressure variations.

The time-depth distribution of the reaction products within and below the decomposition zone may be simulated using DiffMod7. Since secondary mineral reactions and adsorption/desorption are not implemented, the maximum extension of the acid plume is predicted. An estimation of the influences of these processes is difficult, as their importance varies depending on the system of interest. The mineralogical composition – especially the distribution of buffer minerals – and the distribution of sorbed matter might have a great influence. There are several alternative ways of extending DiffMod7 in order to be able to investigate these influences. One possibility is to couple the model to a thermodynamic equilibrium model, such as PHREEQC (Parkhurst and Appelo, 1999). Another way is to combine the diffusion/pyrite-oxidation model DiffMod7 with a transport-reaction model, such as CoTReM (Landenberger, 1998; Adler, 2000), that considers geochemical processes and transport of dissolved products. In both cases, it is questionable if the expected additional results will justify the additional computational effort. Secondary processes, such as the formation of iron and sulfate-storing minerals, are known to have a considerable effect on solute concentrations. However, thermodynamic quantification is difficult due to variable compositions of the minerals and the associated varieties of thermodynamic parameters (e.g. schwertmannite (Yu et al., 1999)). As these secondary minerals are usually meta-stable, they cause a retardation of the transport of primary reaction products by temporarily decreasing solute concentrations. Sorption and desorption, as well as reactions with buffer minerals are of minor importance, especially in mature systems. The release of sodium, potassium, calcium, magnesium, etc. from clay mineral exchange sites results in high solute concentrations, whereas the acid neutralizing effect is small. As these components do not impose any direct hazards, their further behaviour is usually of minor interest. The mobilization of heavy metals or the release of large quantities of aluminium is more important, because of their high eco-toxicity. The behaviour of these components in the course of pyrite decomposition may be well predictable without coupled thermodynamic equilibrium calculations, because of the extreme geochemical settings. For accurate predictions of the behaviour of the different reaction products of pyrite decomposition, and for quantification of subsequent processes, separate calculations using thermodynamic equilibrium models are recommended.

The scope of one-dimensional model calculations is limited. Natural and man-made systems are in general characterized by inhomogeneous structures. Therefore the available data is often just valid over short distances. This fact may be met by an extension of the model to a two-dimensional approach. Many systems characterized by pyrite decomposition processes show complex, however regular structures. In dump bodies of lignite open cast mines, in which conveyor belt bridges are used to transport the overburden material to the dump side of the pit, characteristic depositing structures evolve that strongly influence the soil-physical parameters (Hüttl et al., 2000). Repeating nested structures develop perpendicular to the edge of the pit. Due to the temporal sequence of deposition, different zones of the dump body have been exposed to ambient air for different periods of time. Each period of exposal is associated with the evolvement of a new pyrite decomposition front. As a consequence, different incoher-

ent stages of pyrite decomposition can be found within one dump body, but there is only one currently active decomposition front. This situation is accompanied by a complex distribution of reaction products in seepage water. In order to obtain a basic simulation of these processes and their effects, an extension of the available model to a two-dimensional scheme and a better implementation of seepage water movement is necessary. The higher computational effort would be justified by the very valuable additional information on closer-to-reality systems.

4.5 Summary

The model gives a good insight into the relations between soil-physical parameters, pyrite decomposition rates, seepage water velocity, time, depth and seepage water concentrations in the context of pyrite decomposition processes in the unsaturated zone. The model runs show that the majority of the relevant processes in the examined systems were identified and implemented appropriately. The soil-physical parameters porosity and tortuosity factor, as well as the initial pyrite content of the material are crucial for the release of acid reaction products. Pyrite grain size and pyrite surface, as well as pyrite oxidation rates, are less important for the overall turnover rates and the release of reaction products. Lower reaction rates and/or a smaller amount of available pyrite surface per volume results in an increased thickness of the reaction zone, while the change in release is small. Referring to lignite open mining dumps, material characterised by low permeability and/or low pyrite content should be dumped in locations where increased exposure time is expected. Once more, it is shown that selective dumping must be suggested.

Deviations between model results and chemical analysis of real systems are particularly due to the fact that an implementation of the associated secondary reactions is missing. The model may easily be enhanced by including several other convective transport processes. Moreover, it is suggested to extend the programme towards two-dimensional calculations, in order to give a more accurate picture of real world systems. However, this implies that base data is available at a sufficient level of accuracy.

The programme DiffMod7 was applied to predict the oxygen penetration depth and the associated depyritization depth of a 43 year old dump body. In situ measurements of the oxygen distribution and the determination of pyrite contents within the dump body supported the model results.

One advantage of the model is its ability to run different scenarios to see the effects of different parameter modifications, supporting almost instantaneous graphical feedback. This way, different strategies to prevent or decrease the formation of acid mine drainage may be evaluated and compared.

4.6 References

Adler, M. (2000): Modelling of one-dimensional transport in porous media with respect to simultaneous geochemical reactions in CoTRem. *Ber. FB Geowiss. Univ. Bremen* **166**.

Appelo, C. A. J.; Postma, D. (1994): Geochemistry groundwater and pollution, A. A. Balkema, Rotterdam.

Berner, R. A. (1980): Early Diagenesis: A Theoretical Approach, Princeton Univ. Press, Princeton.

Boudreau, B. P. (1997): Diagenetic Models and Their Implementation – Modelling Transport and Reactions in Aquatic Sediments, Springer-Verlag, Berlin/Heidelberg.

Carman, P. C. (1937): Fluid flow through a granular bed. *Trans. Inst. Chem. Eng.* **15**, 150–156.

Davis, G. B.; Ritchie, A. I. M. (1986): A model of oxidation in pyritic mine wastes 1 – Equations and approximate solution. *Appl. Math. Modell.* **10**, 314–322.

Evangelou, V. P. (1995): Pyrite oxidation and its control, CRC Press Inc., Boca Raton, Florida.

Farrier, D. F.; Massmann, J. (1992): Effects of atmospheric pressure on gas transport in the vadose zone. *Water Resour. Res.* **3**, 777–791.

Friedrich, G.; Dohrmann, R.; Jochum, J.; Echle, W.; Wiechowski, A.; Lang, R.; Riebeiro-Rodrigues, L. C. (1999): Mineralinhalt und Spurenelementverteilung im Neurather Sand – Ihre Bedeutung für die Freisetzung umweltrelevanter Metalle beim Braunkohleabbau im Niederrheinischen Revier. *Z. angew. Geol.* **45**(1), 37–48.

Gerke, H. H.; Molson, J. W.; Frind, E. O. (1998): Modelling the effect of chemical heterogeneity on acidification and solute leaching in overburden mine spoils. *Journal of Hydrology* **209**, 166–185.

Grathwohl, P. (1998): Diffusion in natural porous media: Contaminant Transport, Sorption/Desorption and Dissolution Kinetics, Kluwer Academic Publishers, Bosten/Dordrecht/London.

Hecht, H.;Kölling, M. (accepted): Investigation of pyrite weathering processes in the vadose zone using optical oxygen sensors. *Environmental Geology*.

Holst, G.; Kühl, M.; Klimant, I. (1995): A novel measuring system for oxygen micro-optodes based on a phase modulation technique. *Proc. SPIE* **2508**(45), 387–398.

Hüttl, R. F.; Weber, E.; Klem, D. (Eds.) (2000): Ökologisches Entwicklungspotential der Bergbaufolgelandschaften im Niederlausitzer Braunkohlerevier, B. G. Teubner, Stuttgart/Leipzig/Wiesbaden.

Klein, G. (1935): Handbuch für den deutschen Braunkohletagebau, Verlag W. Knapp, Halle/Saale.

Kölling, M. (1990): Modellierung geochemischer Prozesse im Sickerwasser und Grundwasser. Beispiel: Die Pyritverwitterung und das Problem saurer Grubenwässer. *Ber. FB Geowiss. Univ. Bremen* **8**.

Landenberger, H. (1998): CoTReM, ein Multi-Komponenten Transport- und Reaktions-Modell. *Ber. FB Geowiss. Univ. Bremen* **110**.

Mattheß, G. (1991): Lehrbuch der Hydrogeologie. Band 2: Die Beschaffenheit des Grundwassers, Gebr. Borntraeger, Berlin/Stuttgart.

Mitchell, A. R.; Griffiths, D. F. (1980): The Finite Difference Method in Partial Differential Equations, Wiley, Chichester.

Nordstrom, D. K. (1982): Aqueous pyrite oxidation and the consequent formation of secondary iron minerals. In: Acid sulfate weathering: Pedogeochemistry and Relationship to Manipulation of Soil Materials (Eds.:Kittrick, J. A.; Fanning, D. F.; Hossner, L. R.), Soil Sci. Soc. of America, Madison, Wisconsin. pp. 37–56.

Parkhurst, D. L.; Appelo, C. A. J. (1999): PHREEQC (Version 2) – A computer program for speciation, batch-reaction, one-dimensional transport and inverse geochemical calculations. Water-Resources Investigations Report 99–4259, U.S. Department of the Interior, U.S. Geological Survey, Denver, Colorado.

Prein, A. (1994): Sauerstoffzufuhr als limitierender Faktor für die Pyritverwitterung in Abraumkippen von Braunkohletagebauen. *Mitteilungen, Institut für Wasserwirtschaft, Hydrologie und Landwirtschaftlichen Wasserbau der Universität Hannover* **79**.

Puura, E.; Neretnieks, I.; Kirsimäe K. (1999): Atmospheric oxidation of the pyritic waste rock in Maardu, Estonia – 1. field study and modelling. *Environmental Geology* **39**(1), 1–19.

Schachtschabel, P.; Blume, H.-P.; Brümmer, G.; Hartge, K.-H.; Schwertmann, U. (1992): Scheffer/Schachtschabel: Lehrbuch der Bodenkunde, Ferdinand Enke Verlag, Stuttgart.

Schulz, H. D. (2000): Quantification of Early Diagenesis: Dissolved Constituents in Marine Pore Water. In: Marine Geochemistry (Eds.: Schulz, H. D.; Zabel, M.), Springer-Verlag, Berlin/Heidelberg, pp. 85–128.

Schulz, H. D.; Reardon, E. J. (1983): A combined mixing cell/analytical model to describe two-dimensional reactive solute transport for unidirectional ground water flow. *Water Resour. Res* **19**, 493–502.

Volkov, I. I.; Zhabina, N. N. (1977): Determination of Pyritic Sulfur with Metallic Chromium and Chromium (II) Solution. In: Chemical Analysis of Marine Sediments (Ed.: Ostroumov, E. A.), Nauka, Moscow, pp. 5–14.

Wild, A. (1993): Soil and the environment: an introduction, Cambridge Univ. Press, Cambridge.

Wunderly, M. D.; Blowes, D. W.; Frind, E. O.; Ptacek, C. J. (1996): Sulfide mineral oxidation and subsequent reactive transport of oxidation products in mine tailings impopundments: A numerical model. *Water Resour. Res.* **32**, 3173–3187.

Xu, T.; White, S. P.; Preuss, K. ; Brimhall, G. H. (2000); Modeling of Pyrite Oxidation in Saturated and Unsaturated Subsurface Flow Systems. *Transport in Porous Media* **39**, 25–56.

Yu, J.-Y.; Heo, B.; Choi, I.-K.; Cho, J.-P.; Chang, H.-W. (1999): Apparent solubilities of schwertmannite and ferrihydrite in natural stream waters polluted by mine drainage. *Geochim. Cosmochim. Acta* **63**(19/20), 3407–3416.